Complex conductivity of proximity-superconducting Nb/Cu bilayers

M. S. Pambianchi,* Lie Chen,† and Steven M. Anlage

Center for Superconductivity Research, Department of Physics, University of Maryland, College Park, Maryland 20742

(Received 22 January 1996)

The effective complex conductivity $\sigma^{\mathrm{eff}} = \sigma_1^{\mathrm{eff}} - i\sigma_2^{\mathrm{eff}}$ of proximity-coupled Nb/Cu bilayer films at 11.7 GHz is examined. The peak in the real part $\sigma_1(T)$ just below T_c in bare Nb films gives way to a broader, shallower peak in $\sigma_1^{\mathrm{eff}}(T)$ as the Cu layer thickness increases, consistent with the existence of coherence effects in proximity-superconducting Cu. The imaginary part $\sigma_2^{\mathrm{eff}}(T)$ changes curvature from concave down to concave up as the Cu thickness d_N increases. We extract proximity-induced penetration depth in Cu in the range 320 Å $\leqslant \lambda_N(0,0) \leqslant 580$ Å, with $\lambda_N(0,0)$ increasing slightly with increasing d_N, and an order-parameter decay length in Cu of $K^{-1}(4.6\ \mathrm{K}) = 225$ Å ± 60 Å. The temperature dependence of $K^{-1}(T)$ is consistent with $K^{-1}(T) \sim T^{-2}$. Our results suggest that the single-frequency approximation of Werthamer and de Gennes does not adequately describe the behavior of very thin proximity-coupled Cu layers, in which the exact near-interface profile of the induced order parameter in Cu plays an important role. [S0163-1829(96)06529-0]

Microwave surface impedance measurements provide valuable information about the inhomogeneous superconducting properties of layered systems. In superconductor–normal-metal (S/N) bilayer structures, proximity effects in the normal layer cause altered screening of an applied rf magnetic field and rf loss behavior uncharacteristic of homogeneous superconductors.[1] Such structures have been used previously to mimic the effects of unknown metallic surface layers on the electrodynamics of superconducting samples,[2] as well as to examine the implications of proximity-effect-based theories of cuprate superconductivity.[3]

The Nb/Cu proximity system has been widely studied previously. The well-characterized superconducting properties of Nb and metallic properties of Cu, and the immiscibility of the two at an interface, provide optimum circumstances for studying induced superconductivity in normal metals. Copper samples as thick as 35 μm deposited on Nb have been observed to exclude magnetic fields[4,5] at millkelvin temperatures, and strong flux exclusion by proximity-superconducting Cu at 2 K has been detecting in 1-μm-thick Cu backed by only 550 Å of Nb.[6] Moreover, a true gap in the Cu excitation spectrum in samples proximity-coupled to Pb seems very much in evidence from SNS tunneling measurements.[7] Evidence for case-II coherence effects between excitations above the proximity-induced superconducting ground state has even been reported in NMR measurements on ^{63}Cu in Nb/Cu multilayer samples.[8]

The induced superconducting properties of normal metals in the region near the interface with a superconductor are especially of interest, since very few previous experiments have been sensitive to this region, and since theoretical treatments have been sparse.[9] Fortunately, surface impedance measurements are well suited to studying thin proximity-coupled normal layers, where near-interface properties play a dominant role. The capability of resonant microwave techniques to collect simultaneous information on both the induced superconducting condensate and the set of excitations above that condensate in a proximity-superconducting nor-mal metal enable the present work to fill an important gap in the experimental data on proximity systems.

The induced condensate and the excitations above it are studied individually by considering the effective complex conductivity $\sigma^{\mathrm{eff}} = \sigma_1^{\mathrm{eff}} - i\sigma_2^{\mathrm{eff}}$ of S/N bilayer structures. Upon examining this quantity in proximity-coupled Nb/Cu bilayers, we find a broad peak in the real part of σ_1^{eff} at $T/T_c \sim 0.3$–0.5 and a change in curvature of $\sigma_2^{\mathrm{eff}}(T)$ as $T \to 0$ for Cu thicknesses $d_N > 270$ Å. We show that these behaviours are associated with coherence effects between excitations above the induced condensate in proximity-superconducting Cu and with the divergence of the order-parameter decay length $K^{-1}(T)$ in Cu, respectively. Moreover, both the order-parameter decay length K^{-1} and the induced normal layer penetration depth $\lambda_N(0,0)$ in Cu are much smaller than values found previously in thicker Cu layers, and the divergence of $K^{-1}(T)$ as $T \to 0$ is closely approximated by $K^{-1}(T) \sim T^{-2}$, rather than the T^{-1} or $T^{-1/2}$ temperature dependences reported earlier.[4,5] These results suggest that the single-frequency approximation,[10,11] which has been applied successfully to proximity effect phenomena far from the S/N interface, is insufficient for describing the behavior of thin proximity-coupled Cu layers.

Proximity-coupled Nb/Cu bilayer films were prepared on 3″ diameter Si(100) wafers by dc magnetron sputtering in 4 mTorr flowing argon, after first attaining a chamber base pressure of 4×10^{-8} Torr. Their geometry is shown in the inset of Fig. 1. First, Nb was deposited to a thickness $d_s = 3000$ Å at 450 ° C using 1200 W power on a 3″ diameter high-purity Nb target, after which the substrate was cooled *in situ* before depositing Cu at 100° C using 1000 W power on a 3″ high-purity Cu target. The thicknesses d_N of the Cu layers ranged from 90 to 760 Å. Bare Nb films prepared in this manner had resistivities in the range $\rho(10\ \mathrm{K}) \approx 0.5$–$1.0$ $\mu\Omega$ cm, with residual resistivity ratio $\rho(300\ \mathrm{K})/\rho(10\ \mathrm{K}) \approx 6$, while 2000 Å-thick bare Cu films showed $\rho(10\ \mathrm{K}) \approx 0.2$ $\mu\Omega$ cm and $\rho(300\ \mathrm{K})/\rho(10\ \mathrm{K}) \approx 10$. Bilayers showed superconducting transition temperatures in the range 8.7 K $< T_c < 9.0$ K in dc resistance measurements.
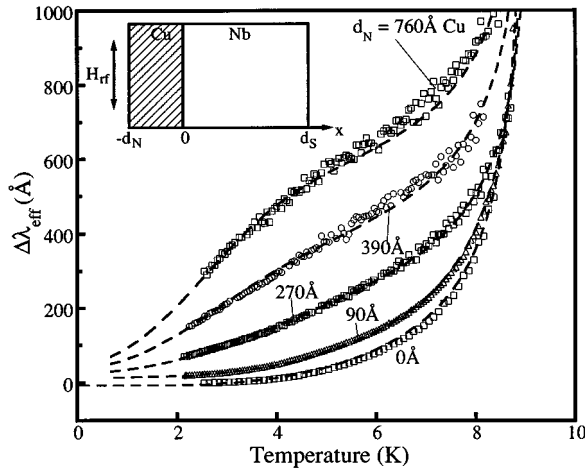
FIG. 1. Change in effective penetration depth $\Delta\lambda_{eff}(T)$ for Nb/Cu bilayers. The curves have been offset arbitrarily in the vertical direction for clarity. The dashed curves are fits to the proximity electrodynamics model presented in the text, using the temperature dependence of the order-parameter decay length $K^{-1}(T)\sim T^{-2}$. The fit to bare Nb data uses the temperature dependence given by Mühlschlegel (see Ref. 15), with parameters $\lambda(0)=350$ Å, $T_c=9.17$ K. Inset: Proximity-superconducting bilayer geometry.

Surface impedance measurements on Nb/Cu bilayers were performed at 11.7 GHz using a parallel-plate resonator.[1,12,13] In this technique, two identical bilayer films are placed face to face and separated by a dielectric material of thicknesses[14] $d=12.5$ μm, forming a transmission line supporting TEM electromagnetic waves. The resonant frequency f and quality factor Q of such a transmission line are related to magnetic-field penetration and rf loss in the superconducting plates, respectively. Changes in resonant frequency f are caused by changes in the inductance per unit length $\mathbf{L}$; we may define an effective penetration depth λ_{eff} by $\mathbf{L}=(\mu_0/W)[d+2\lambda_{eff}]$, where W is the film width, and where λ_{eff} includes effects associated with nonexponential screening, including the proximity effect and finite thickness effects. Since $f\sim\mathbf{L}^{-1/2}$, changes in λ_{eff} cause the resonant frequency to shift according to $\Delta\lambda_{eff}=\lambda_{eff}(T)-\lambda_{eff}(T_0)=(d/2)\{[f(T_0)/f(T)]^2-1\}$, where T_0 is the lowest temperature at which data is taken. For thick single-layer superconducting films, it can be shown that λ_{eff} equals the superconducting penetration depth λ, owing to the exponential penetration of magnetic field. Though in proximity-coupled S/N bilayers λ_{eff} does not correspond to any single screening length scale, changes in this quantity $\Delta\lambda_{eff}$ can be compared directly with changes $\Delta\lambda$ for bare superconducting films, which have a well-known temperature dependence. In this way, the departure from homogeneous superconducting behavior in proximity-effect bilayers can be quantified.

The effective penetration depth change $\Delta\lambda_{eff}$ is shown vs temperature in Fig. 1 for samples with Cu thicknesses $d_N=0$, 90, 270, 390, and 760 Å, all grown on 3000 Å-thick Nb. A systematic change in the temperature dependence of $\Delta\lambda_{eff}$ was observed with increasing Cu thickness. For $d_N=0$ Å, the bare Nb sample obeyed the BCS temperature dependence[15] very closely, with fitting parameters $\lambda_s(0)=350$ Å and $T_c=9.17$ K. With Cu layers of thickness
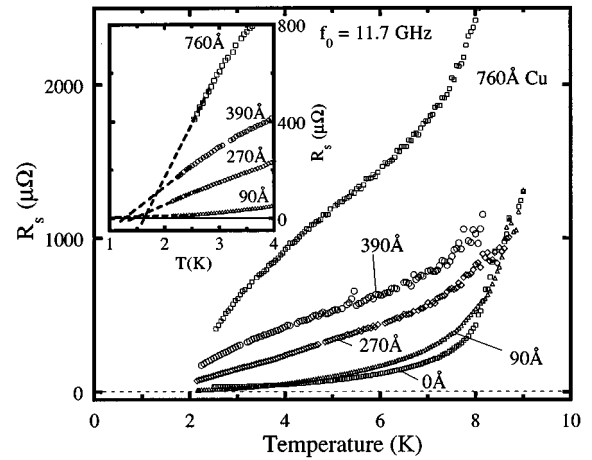

FIG. 2. Surface resistance $R_s(T)$ for Nb/Cu bilayers at 11.7 GHz, corrected for extrinsic losses. Note that the sample with 90 Å Cu has lower R_s at 2.5 K than the bare Nb sample. Inset: Low-temperature linear extrapolations of $R_s(T)$ for Nb/Cu bilayers, showing increase of dR_s/dT with d_N.

90 and 270 Å, a nonexponential approach of $\Delta\lambda_{eff}$ to a constant value as $T\rightarrow0$ was noticeable. For $d_N=390$ Å, a linear dependence of $\Delta\lambda_{eff}$ on temperature persisted up to 8 K, while for $d_N=760$ Å a change in curvature and more rapid drop in $\Delta\lambda_{eff}$ occurred as $T\rightarrow0$, described by $\Delta\lambda_{eff}(T)\sim T^{\alpha}$, with $\alpha\lesssim1$. Fits to the model described below are also shown in Fig. 1 as dashed lines.

The surface resistance data, inversely related[16] to the measured quality factor Q are shown in Fig. 2. Behavior similar to that of the $\Delta\lambda_{eff}$ data is apparent; at $d_N=0$ Å the surface resistance approach its low-temperature residual value (22 $\mu\Omega$) exponentially slowly as expected from the BCS theory;[17] Mattis-Bardeen[18,19] fits using $2\Delta(0)/k_BT_c=3.5$ yielded a normal-state conductivity of $\sigma_{Nb}=1.37\times10^8$ Ω^{-1} m^{-1}, in agreement with dc resistivity results at 10 K. For $d_N=90$ Å, a Mattis-Bardeen-like temperature dependence also was observed as $T\rightarrow0$, but with a much smaller residual surface resistance value (less than 10 $\mu\Omega$). This smaller residual R_s is probably due to a passivation effect in which Cu prevented oxide formation in the underlying Nb. For thicknesses $d_N=270$, 390, and 760 Å, $R_s(T)\sim T$ was observed at low temperatures, with a characteristic curvature change and rapid drop as $T\rightarrow0$ occurring in the two thickest samples, just as in the $\Delta\lambda_{eff}$ data. The magnitude of R_s and slope dR_s/dT at low temperature increased monotonically with increasing d_N (except for the 90 Å case at low T), and linear extrapolations of $R_s(T)$ to below 2 K intercept zero at temperatures which generally increase with increasing Cu thickness (see inset of Fig. 2).

The conversion of these data to real and imaginary parts of the effective conductivity (σ_1^{eff} and σ_2^{eff}, respectively) allows one to examine the properties of the proximity-induced condensate (σ_2^{eff}) and the excitations above this condensate (σ_1^{eff}) independently. The effective conductivities were obtained according to the local limit expression $Z_s=R_s+iX_s=[i\omega\mu_0/(\sigma_1^{eff}-i\sigma_2^{eff})]^{1/2}$, where $X_s=\mu_0\omega\lambda_{eff}$, analogous to expressions for a homogeneous superconductor. No residual surface resistance was subtracted from R_s when

TABLE I. Effective penetration depths $\lambda_{\text{eff}}(T_0)$, with lower and upper bounds, used to calculate real and imaginary parts of the conductivity for Nb/Cu bilayers.

d_N (Å)	$\lambda_{\text{eff}}^{\text{model}}(T_0)$ (Å)[a]	$d_N + \lambda_{\text{Nb}}(T_0)$ (Å)[b]	$\lambda_{\text{eff}}(T_0)$ (Å)
0	350	350	350
90	380	440	410
270	490	620	550
390	590	740	660
760	950	1140	1040

[a]Lower bound for $\lambda_{\text{eff}}(T_0)$, calculated using $\lambda_N(0,0) = 300$ Å, K^{-1} (4.6 K) = 225 Å, and $\lambda_{\text{Nb}}(0) = 350$ Å.
[b]Upper bound for $\lambda_{\text{eff}}(T_0)$ (assumes the normal layer does no screening).

calculating σ_1^{eff} and σ_2^{eff}. Since only changes in λ_{eff} could be measured, values of λ_{eff} were chosen at the lowest temperature T_0 measured for each sample using the following method. $\lambda_{\text{eff}}(T_0)$ was chosen as the average of the value of λ_{eff} calculated by an electrodynamics model[2] described below and the value of the sum $d_N + \lambda_{\text{Nb}}(T_0)$. The model calculation was taken to be a lower limit for $\lambda_{\text{eff}}(T_0)$, since the parameters used in it ($\lambda_N(0,0) = 300$ Å, K^{-1}(4.6 K) = 225 Å, $\lambda_{\text{Nb}}(0) = 350$ Å) represent underestimates[20] for proximity-coupled Cu. The latter quantity is the upper limit for $\lambda_{\text{eff}}(T_0)$, in which the rf magnetic field simply penetrates through the Cu layer unperturbed and is screened by the Nb layer. Table I shows the values of $\lambda_{\text{eff}}(T_0)$ used, as well as the lower and upper limits.

Figure 3 shows the real part $\sigma_1^{\text{eff}}(T)$ for Nb/Cu bilayers. While bare Nb correctly exhibits the well-characterized BCS coherence peak at $T \sim 7$ K, followed by an exponential tail as $T \to 0$, proximity-coupled Nb/Cu samples show lesser peaks in $\sigma_1^{\text{eff}}(T)$ occurring at temperatures which decrease as d_N increases. While most of the coherence peak of the underlying Nb is still visible with very thin Cu cover layers, all traces of this peak gradually become obscured by screening activity in the Cu layer as d_N increases. It is useful to note
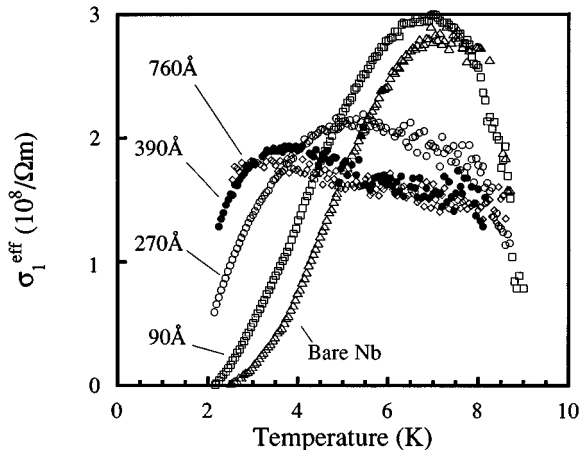

FIG. 3. Real part $\sigma_1^{\text{eff}}(T)$ of the complex conductivity of Nb/Cu bilayers at 11.7 GHz, showing the peak which occurs at lower temperature with increasing d_N.
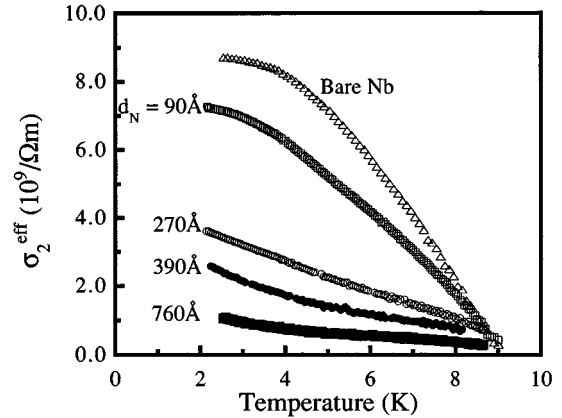

FIG. 4. Imaginary part $\sigma_2^{\text{eff}}(T)$ of the complex conductivity of Nb/Cu bilayers at 11.7 GHz, showing the change in curvature with increasing d_N. The choice of $\lambda_{\text{eff}}(T_0)$ required to construct $\sigma_2^{\text{eff}}(T)$ is discussed in the text.

that using the lower or the upper limits for $\lambda_{\text{eff}}(T_0)$ given in Table I, rather than the average of the two, does not substantially alter the shape of the curves in Fig. 3.

Figure 4 displays the imaginary part $\sigma_2^{\text{eff}}(T)$, which characterizes properties of the superconducting condensate in the bilayer. Here the behavior of Nb/Cu bilayers is also unique; in Nb, $\sigma_2^{\text{eff}}(T)$ approaches a constant value exponentially slowly as $T \to 0$ as predicted by BCS theory, while in Nb/Cu bilayers $\sigma_2^{\text{eff}}(T)$ changes curvature and continues to increase as $T \to 0$. The Cu thickness at which this curvature change becomes apparent is $d_N = 270$ Å, for which $\sigma_2^{\text{eff}}(T) \sim 1 - T/T_c$. The crossover from BCS-like to non-BCS-like behavior at $d_N = 270$ Å suggest that 270 Å is approximately equal to some characteristic screening length in proximity-superconducting Cu.

The upturn in $\sigma_2^{\text{eff}}(T)$ as $T \to 0$ in the thicker Cu samples signals the onset of induced screening in the Cu layers caused by divergence of the order-parameter decay length $K^{-1}(T)$. This upturn becomes more abrupt as d_N increases, since appreciable proximity-induced screening only occurs when $K^{-1} \sim d_N$. Since $K^{-1}(T)$ diverges as $T \to 0$, it passes through the value of d_N more rapidly and at a lower temperature when d_N is larger. We estimate K^{-1}(4.6 K) = 225 Å ± 60 Å by comparing with model calculations described below. We also note that these conclusions do not depend on our choice of $\lambda_{\text{eff}}(T_0)$; the shapes of the curves $\sigma_2^{\text{eff}}(T)$ are not substantially altered by choosing different values for $\lambda_{\text{eff}}(T_0)$ within the range of possible values given in Table I.

The model of electrodynamics in proximity-superconducting systems used in this work has been established in two earlier publications.[1,2] In summary, it assumes an exponentially varying penetration depth $\lambda_N(x,T) \sim \lambda_N(0,T)e^{K(T)|x|}$ in the normal layer, corresponding to the decaying order parameter in the proximity-coupled normal metal (note the x axis defined in the inset of Fig. 1). The decay length scale $K^{-1}(T)$ grows rapidly[21] near the superconducting transition temperature T_{cN} of the N metal (we take $T_{cN} = 0$ K for Cu). Maxwell's equations are solved using a generalized London equation which contains the spatially inhomogeneous penetration depth $\lambda_N(x,T)$, yielding

TABLE II. Normal-metal layer thicknesses and fitting parameters for $\Delta\lambda_{\text{eff}}(T)$ data on Nb/Cu bilayers (Fig. 1), using the temperature dependence $K^{-1}(T) \sim T^{-2}$ for the decay length.

d_N (Å)	$\lambda_N(0,0)$ (Å)	K^{-1} (4.6 K) (Å)	$\lambda_S(0)$ (Å)	T_c (K)
90	470 ± 40	225 ± 10	400 ± 50	9.3 ± 0.05
270	318 ± 15	227 ± 15	300 ± 50	9.3 ± 0.05
390	363 ± 20	160 ± 20	350 ± 50	9.3 ± 0.05
760	578 ± 40	285 ± 23	340 ± 20	9.3 ± 0.05

expressions for the magnetic field $H(x,T)$ and the supercurrent $J_s(x,T)$. From these the total (magnetic and kinetic) inductance per unit length and the resonant frequency of a parallel-plate resonator can be calculated.[2] To calculate the surface resistance, the model assumes a local value of the BCS gap $\Delta_N(x,T) = \Delta_N(0,T)e^{-K(T)|x|}$ in the normal metal possessing the same exponential decay length scale as $\lambda_N(x,T)$. This local gap is used to calculate the local BCS real part of the conductivity $\sigma_1 = \sigma_1(\Delta_N(x,T),\omega,T)$, using the Mattis-Bardeen theory,[18] from which the surface resistance is in turn calculated. Throughout, the model treats the Nb layer as an unperturbed BCS superconductor.[2] This model, through nonrigorous, was shown to correctly describe both $\Delta\lambda_{\text{eff}}(T)$ and $R_s(T)$ in Nb/Al bilayers.[1]

The temperature dependence $K^{-1}(T) \sim T^{-2}$ was found to produce close agreement with the $\Delta\lambda_{\text{eff}}(T)$ data, rather than the $K^{-1}(T) \sim T^{-1/2}$ or $K^{-1}(T) \sim T^{-1}$ dependences predicted by clean- and dirty-limit single-frequency approximation expressions.[21] Using $l = 3950$ Å for Cu, derived from resistivity measurements using[22] $\rho l = 7.9 \times 10^{-16}$ Ω m^2, these expressions reduce to $K_{\text{dirty}}^{-1}(T) = 2410$ Å (4 K/T)$^{1/2}$ and $K_{\text{clean}}^{-1}(T) = 4770$ Å (4 K/T). However, the single-frequency approximation applies only to regions of the normal metal far from the S/N interface, i.e., $|x| \gg K^{-1}$, and approximates the rapid spatial variation of the order parameter near the interface with a discontinuity there. As such it contains no description of the true behavior of the order parameter in the normal layer near the S/N interface. Since even the thickest Cu sample ($d_N = 760$ Å) presented here is thinner than the predicted dirty-limit value of K^{-1}, the precise spatial dependence of the order parameter near the S/N interface may be very different from that predicted by the single-frequency approximation. The observed T^{-2} temperature dependence does not emerge from the single-frequency approximation theories under any circumstances, though it has been observed before in magnetization[23] and ac susceptibility[24] experiments on other low-T_c proximity systems. These results suggest that the near-interface profile of the induced order parameter in Cu, which is neglected in the single-frequency approximation, must be considered fully in order to reproduce observed data on such thin normal layers.

The fits to the $\Delta\lambda_{\text{eff}}(T)$ data are shown in Fig. 1. They describe the data remarkably well, reproducing both the linear portions of $\Delta\lambda_{\text{eff}}(T)$ at low temperature for the thinner Cu samples ($d_N = 90$ Å, 270 Å) and the change of curvature for the thicker Cu samples ($d_N = 390$ Å, 760 Å). The parameter values for $\lambda_N(0,0)$ and K^{-1} (4.6 K) yielding the best fits to $\Delta\lambda_{\text{eff}}(T)$ are given in Table II; these agree well across all

of the samples. The error bars quoted after each value reflect the size of the variation which produced a 5% reduction in fit quality.

Apart from the 90 Å data, it can be discerned that the values of $\lambda_N(0,0)$ increase with d_N. This has been noted before in magnetization measurements[23] and is even apparent, though not explicitly discussed, in the work of Simon and Chaikin.[25] Moreover, the range of values 320 Å $\leq \lambda_N(0,0) \leq 580$ Å put $\lambda_N(0,0)$ much closer to the London value of $\lambda_L = 200$ Å for Cu than previous experimental results on thicker normal-metal layers, which always yielded penetration depths significantly larger than the London value [$\lambda_N(0,0) = 1500$ Å vs $\lambda_L = 250$ Å in Ag,[25] and $\lambda_N(0,0) = 900$ Å vs $\lambda_L = 500$ Å in Al,[25] $\lambda_N(0,0) = 1040$ Å vs $\lambda_L = 200$ Å in Cu (Ref. 26)] even at the lowest temperatures. Both of these pieces of evidence fit naturally into a picture in which the induced order parameter in Cu varies rapidly near the S/N interface. While the exact near-interface behavior is unimportant for thick normal layers ($d_N \gg K^{-1}$), it dominates the characteristics of a thin normal layer, and, unlike thick normal layers, may itself be a function of the normal layer thickness d_N. Clearly characteristic length scales such as $\lambda_N(0,0)$ and K^{-1}(4.6 K) could vary with normal layer thickness as well when the normal layer is thin. The relatively short induced penetration depths in thin normal layers also would reflect the larger induced order parameter near the S/N interface, which would extend over more of the normal layer if it were thin.

In order to gain more insight into the rf losses of proximity-coupled bilayers we used the model to calculate profiles of the screening current J, effective resistivity $\rho^{\text{eff}} = \sigma_1(x,T)/\{\sigma_1^2(x,T) + [1/\mu_0\omega\lambda^2(x,T)]^2\}$, and local loss $\rho^{\text{eff}}J^2$ in the 760 Å Cu/3000 Å Nb samples, using parameters $\lambda_N(0,0) = 300$ Å, K^{-1}(4.6 K) $= 150$ Å, $\lambda_{\text{Nb}}(0) = 350$ Å, $\sigma_N(\text{Nb}) = 1.37 \times 10^8$ Ω^{-1} m^{-1}, and $\sigma_N(\text{Cu}) = 2.74 \times 10^8$ Ω^{-1} m^{-1}. These profiles across the thickness of the bilayer are shown in Fig. 5 for $T = 1$, 2, 4, and 8 K. The screening current, shown in Fig. 5(a), always flows where larger order parameter exists, namely, near the S/N interface. Because of the diverging decay length $K^{-1}(T)$, however, the local effective resistivity has a maximum in the middle of the Cu layer at 8 K which gradually moves to the free surface as the temperature is lowered, as shown in Fig. 5(b). The consequence is that the local loss contribution given by the product $\rho^{\text{eff}}J^2$ has a maximum at the S/N interface at 8 K which moves into the middle of the Cu layer and eventually to the free surface as the temperature decreases to 1 K. The surface resistance is given by the area under each curve in Fig. 5(c).

The profiles in Fig. 5 are central to understanding the $\sigma_1^{\text{eff}}(T)$ peaks of Fig. 3, which were originally thought to be related only to a shift in the location of screening currents caused by the onset of proximity-induced superconductivity in Cu. It is clear that, with the reasonable parameters used to generate Fig. 5, the screening currents need not shift spatially very much with temperature. Rather, the spatial distribution of quasiparticle excitations may be strongly temperature dependent, leading to a shift in the position inside the normal layer where most of the loss occurs.

The remaining point concerns correlations between such normal excitations, which in a homogeneous superconductor are described by case-II coherence factors.[27] To explore this
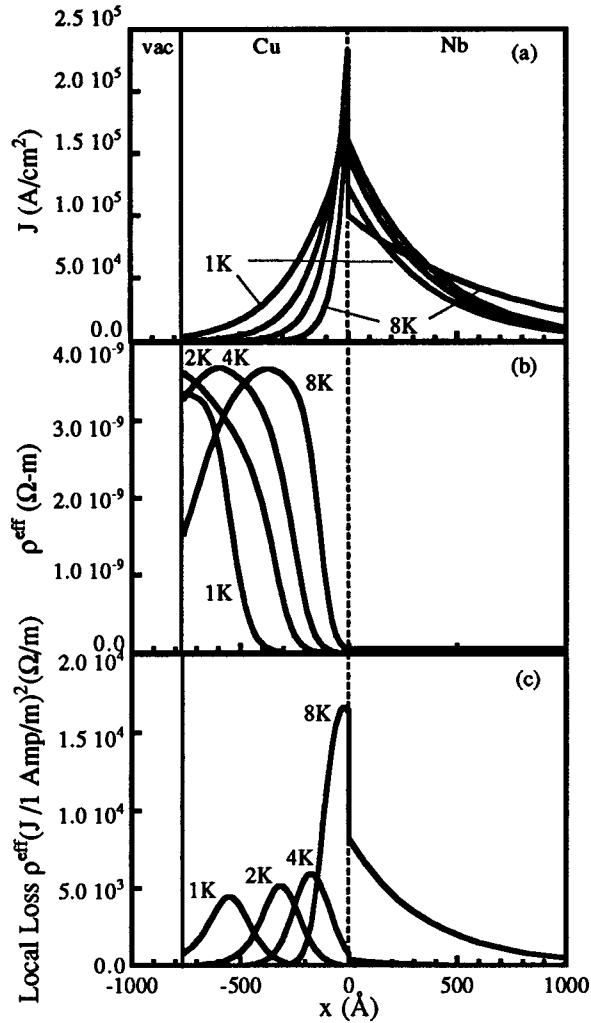
FIG. 5. (a) Model calculations of the current density profile across the thickness of a proximity-coupled 760 Å Cu/3000 Å Nb bilayer film at 1, 2, 4, and 8 K, using the same parameters as in Fig. 6. (b) Local effective rf resistivity profile at 11.7 GHz at 1, 2, 4, and 8 K, using the normal-state conductivities used in Fig. 6, with coherence effects in Cu included. (c) Local loss profile $\rho^{\mathrm{eff}}(x)J^2(x)$ in Ω/m (assuming a surface field of 1 A/m) at 1, 2, 4, and 8 K. The surface resistance R_s at each temperature is represented by the area under the corresponding curve in (c).

FIG. 6. Model calculations of $\sigma_1^{\mathrm{eff}}(T)$, using $d_N = 270$ Å, $\lambda_N(0,0) = 300$ Å, $K^{-1}(4.6\text{ K}) = 225$ Å, $\lambda_{\mathrm{Nb}}(0) = 350$ Å, σ_N (Nb) $= 1.37 \times 10^8$ Ω^{-1} m^{-1}, σ_N (Cu) $= 2.74 \times 10^8$ Ω^{-1} m^{-1}, including coherence effects in Cu (dashed line) and without coherence effects in Cu (solid line). Data for the 270 Å Cu/3000 Å Nb and 390 Å Cu/3000 Å Nb samples are included for comparison.

concept further, a second loss model was created in which the local Mattis-Bardeen conductivity in the N layer was replaced with a two-fluid conductivity expression, given simply by the fraction of normal excitations at temperature T thermally excited over the local gap $\Delta_N(x,T)$ multiplied by the normal-state conductivity of the N layer. This model thus contains no mention of case-II coherence effects, though it preserves the concept of a diverging order-parameter decay length and an activation barrier for quasiparticle excitation.

A comparison of the two models in Nb/Cu bilayers is shown with the $\sigma_1^{\mathrm{eff}}(T)$ data for the 270 and 390 Å samples in Fig. 6. The upper of the two calculated curves was generated using the full Mattis-Bardeen-based model including coherence effects in Cu, while the lower curve was generated with the second model containing no coherence effects in
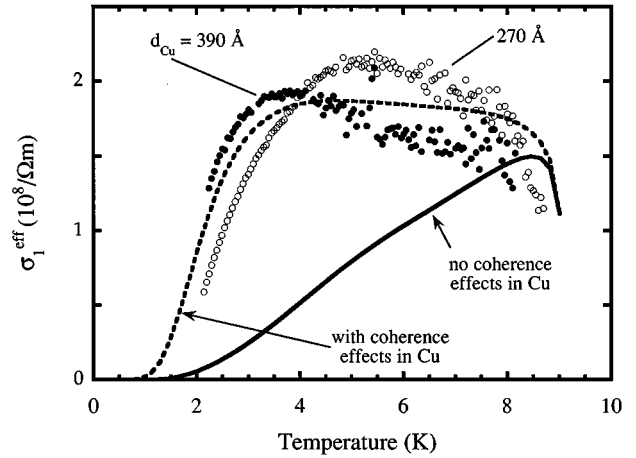
Cu. Although neither curve fits the data precisely, it was found after much effort that it was not possible to reproduce any feature remotely resembling the low-temperature peak in $\sigma_1^{\mathrm{eff}}(T)$ using the model without coherence effects. We conclude that the low-temperature peaks in $\sigma_1^{\mathrm{eff}}(T)$ shown in Fig. 3 represent evidence that coherence effects play a role in the electrodynamics of proximity-superconducting Cu. The peaks are shallower and broader because the Cu becomes superconducting more gradually via the proximity effect than a homogeneous superconductor does at its transition temperature. Such a peak implies a peak in the density of states of the normal metal, a ''gaplike'' feature. Interestingly, this is consistent with calculations of the density of states $N(\varepsilon)$ in the normal layers of S/N/S multilayers by Golubov.[28]

In summary, we have examined the behavior of the induced condensate and the normal excitations above it in proximity-superconducting Nb/Cu bilayer films. The BCS coherence peak in σ_1 in Nb bare films gives way to a broad, smaller peak in σ_1^{eff} occurring at lower temperatures as the Cu thickness is increased; our work presents compelling evidence that this is associated with superconducting coherence effects in Cu. We infer parameter values 320 Å $\leqslant \lambda_N(0,0) \leqslant 580$ Å and $K^{-1}(4.6\text{ K}) = 225$ Å± 60 Å for Cu from fitting the near-interface order-parameter decay length to the temperature dependence $K^{-1}(T) \sim T^{-2}$. From these values and this temperature dependence we conclude that the single-frequency approximation is not adequate for describing the rapid variation of the order parameter near the S/N interface in thin proximity-coupled normal metals.

*Present address: HYPRES, Inc. 175 Clearbrook Road, Elmsford, New York 10523.

†Permanent address: Chinese Academy of Sciences, Institute of Physics, National Laboratory for Superconductivity, P. O. Box 603, Beijing 100080, China.

[1] M. S. Pambianchi, S. N. Mao, and S. M. Anlage, Phys. Rev. B **52**, 4477 (1995).

[2] M. S. Pambianchi, J. Mao, and S. M. Anlage, Phys. Rev. B **50**, 13 659 (1994).

[3] V. Z. Kresin and S. A. Wolf, Phys. Rev. B **46**, 6458 (1992); R. A. Klemm and S. H. Liu, Phys. Rev. Lett. **74**, 2343 (1995).

[4] Y. Oda, A. Sumiyama, and H. Nagano, Jpn. J. Appl. Phys. **22**, 464 (1983).

[5] A. C. Mota, in *Josephson Effect-Achievement and Trends*, edited by A. Barone (World Scientific, Singapore, 1986), p. 248.

[6] J. H. Claasen, J. E. Evetts, R. E. Somekh, and Z. H. Barber, Phys. Rev. B **44**, 9605 (1991).

[7] J. Clarke, Proc. R. Soc. London Ser. A **308**, 447 (1969).

[8] G. Q. Zheng, Y. Kohori, Y. Oda, K. Asayama, R. Aoki, Y. Obi, and H. Fujimori, J. Phys. Soc. Jpn. **58**, 39 (1989).

[9] W. Silvert, J. Low Temp. Phys. **20**, 439 (1975).

[10] N. R. Werthamer, Phys. Rev. **132**, 2440 (1963).

[11] P. G. de Gennes, Rev. Mod. Phys. **36**, 225 (1964).

[12] R. C. Taber, Rev. Sci. Instrum. **61**, 2200 (1990).

[13] M. S. Pambianchi, S. M. Anlage, E. S. Hellman, E. H. Hartford, Jr., M. Bruns, and S. Y. Lee, Appl. Phys. Lett. **64**, 244 (1994).

[14] The spacer is made of Teflon FEP, and its thickness for the bilayer sample with the thickest Cu layer (760 Å) was 75 μm; all others were 12.5 μm thick.

[15] B. Mühlschlegel, Z. Phys. **155**, 313 (1959).

[16] The expression relating Q and R_s is $1/Q = R_s/(\pi \mu_0 f d) + (1/Q_{ff}) + \tan\delta$, where Q_{ff} is a measure of the energy lost via coupling through the fringing fields at the edges of the resonator, and $\tan\delta$ quantifies the dielectric loss. Weak coupling is assumed, so that any additional term $1/Q_{coupling}$ may be neglected. Q_{ff} and $\tan\delta$ were determined by varying the thickness of the spacer over the range 12.5 μm$\leq d \leq$125 μm. By fitting d/Q to a quadratic function of d, these extrinsic sources of loss were extracted and accounted for. See Ref. 12.

[17] J. P. Turneaure, J. Halbritter, and H. A. Schwettman, J. Supercond. **4**, 341 (1991).

[18] D. C. Mattis and J. Bardeen, Phys. Rev. **111**, 412 (1958).

[19] In the fits of $R_s(T)$ data for bare Nb to Mattis-Bardeen theory, we assume that there is a temperature-independent residual resistance of 22 $\mu\Omega$.

[20] The proximity-induced penetration depth in Cu cannot be less than the London penetration depth $\lambda_L = 200$ Å, the value calculated from the electron density and effective mass in Cu. The smallest penetration depth obtained from fitting to the electrodynamic model (below) was found to be $\lambda_N(0,0) = 320$ Å, so 300 Å was ultimately used as a lower bound.

[21] If the single-frequency approximation is used, the order-parameter decay length is given in the dirty and clean limits by $K^{-1}(T) = (\hbar v_F l / 6\pi k_B T)^{1/2}$ and $K^{-1}(T) = \hbar v_F / 2\pi k_B T$, respectively, where v_F is the Fermi velocity, and l is the mean free path.

[22] The Drude resistivity can be written as $\rho l = \mu_0 v_F \lambda_L^2$, and using $v_F = 1.57 \times 10^6$ m/s and $\lambda_L = 200$ Å for Cu gives $\rho l = 7.9 \times 10^{-16}$ Ω m².

[23] A. C. Mota, P. Visani, and A. Pollini, J. Low Temp. Phys. **76**, 465 (1989).

[24] M. L. Wilson and J. H. Claasen, Bull. Am. Phys. Soc. **40**, 72 (1995).

[25] R. W. Simon and P. M. Chaikin, Phys. Rev. B **23**, 4463 (1981); **30**, 3750 (1984).

[26] E. Krätzig and W. Schreiber, Phys. Kondens. Mater. **16**, 95 (1973).

[27] M. Tinkham, *Introduction to Superconductivity* (McGraw-Hill, New York, 1975), p. 57.

[28] A. A. Golubov, SPIE Proc. **2157**, 353 (1994).